DALTON

Thiolateisocyanide complexes of molybdenum(II) and tungsten(II): crystal structures of *cis*-[Mo(SC$_6$H$_2$Pr$^i_3$-2,4,6)$_2$(CNMe)$_4$], *cis*-[Mo(SC$_6$H$_2$Pr$^i_3$-2,4,6)$_2$(CNBu^t)$_4$] and *cis*-[W(SC$_6$H$_2$Pr$^i_3$-2,4,6)$_2$(CNMe)$_4$], and anodically induced isomerisation studies

M. Fatima C. Guedes da Silva,[a] Peter B. Hitchcock,[b] David L. Hughes,[c] Katayoun Marjani,[b] Armando J. L. Pombeiro *,[a] and Raymond L. Richards *,[c]

[a] *Centro de Química Estrutural, Complexo I, Instituto Superior Técnico, Av. Rovisco Pais, 1096 Lisboa codex, Portugal*
[b] *School of Chemistry, Physics and Environmental Science, University of Sussex, Brighton, UK BN1 9QJ*
[c] *John Innes Centre, Nitrogen Fixation Laboratory, Colney Lane, Norwich, UK NR4 7UH*

Reaction of [MH(SC$_6$H$_2$Pr$^i_3$-2,4,6)$_3$(PMe$_2$Ph)$_2$] (M = Mo or W) or [MoH(SC$_6$H$_2$Pr$^i_3$-2,4,6)$_3$(PMePh$_2$)] with RNC (R = Me or Bu^t) gave the complexes *cis*-[M(SC$_6$H$_2$Pr$^i_3$-2,4,6)$_2$(CNR)$_4$] **1** (M = Mo, R = Me or Bu^t; M = W, R = Me), which have been shown to have distorted octahedral geometry by X-ray crystallography. Spectroscopic data for **1** are also described. At −50 °C in CH_2Cl_2 solution the complexes *cis*-[Mo(SC$_6$H$_2$Pr$^i_3$-2,4,6)$_2$(CNR)$_4$] (R = Me or Bu^t) undergo an anodically induced isomerisation according to an electrochemical–chemical square-type mechanism for which rate and equilibrium constants have been estimated by digital simulation of cyclic voltammetric data.

Following our interest in the reactivity of sulfur-ligated complexes which relate to catalytic processes such as nitrogen fixation and hydrodesulfurisation [1,2] we have described the reactions of the electron-deficient complexes [MH(SC$_6$H$_2$Pr$^i_3$-2,4,6)$_3$(PMe$_2$Ph)$_2$] (M = Mo or W) and [MoH(SC$_6$H$_2$Pr$^i_3$-2,4,6)$_3$(PMePh$_2$)] [1] with nitrogen-donor ligands to give adducts such as [MoH(SC$_6$H$_2$Pr$^i_3$-2,4,6)$_3$(PMePh$_2$)(C$_5$H$_5$N)],[2] with CO to give [Mo(SC$_6$H$_2$Pr$^i_3$-2,4,6)$_2$(CO)$_3$(PMePh$_2$)] and [M(SC$_6$H$_2$Pr$^i_3$-2,4,6)$_2$(CO)$_2$(PMe$_2$Ph)$_2$],[3] with PhC≡CH in MeOH to give [MoO(SC$_6$H$_2$Pr$^i_3$-2,4,6)$_3${=C(Ph)CH=C(Ph)CH$_2$PMe$_2$Ph}] [4] and thermally to give S–C cleavage reactions.[5] Here we describe an extension of these studies to the reactions of these hydridethiolates with isocyanide ligands, which result in the reductive elimination of thiol and loss of phosphine from the co-ordination sphere of the metal to give new six-co-ordinate, d^4, thiolateisocyanide complexes whose distorted octahedral structures have been demonstrated by crystal structure determination.

Moreover, in view of the known dependence of the molecular geometry of co-ordination compounds on their electronic configuration,[6] mainly investigated [7–18] for *cis* and *trans* isomers of octahedral-type redox pairs with 18-/ 17-/ 16-electrons (the last ones in a much lesser number of cases), a subject of considerable debate which has been attracting our attention,[9] we have also studied in detail by digital simulation, as described below, the electrochemical behaviour of the 16-electron complexes *cis*-[Mo(SC$_6$H$_2$Pr$^i_3$-2,4,6)$_2$(CNR)$_4$] (R = Me or Bu^t). We have found that at low temperature they isomerise upon a single-electron oxidation. This is an extension (which also provides the first detailed kinetic investigation) of the rather limited range of studies [11,13] of electron-transfer-induced rearrangements in 16-/ 15-electron redox-pair systems.

Results and Discussion

Preparation and structural studies of *cis*-[M(SC$_6$H$_2$Pr$^i_3$-2,4,6)$_2$(CNR)$_4$] 1 (M = Mo, R = Me or Bu^t; M = W, R = Me)

Reaction of the five-co-ordinate complex [MoH(tipt)$_3$(PMePh$_2$)] (tipt = SC$_6$H$_2$Pr$^i_3$-2,4,6) and the six-co-ordinate complexes [WH(tipt)$_3$(PMe$_2$Ph)$_2$] and [MoH(tipt)$_3$(PMe$_2$Ph)$_2$] with an excess of isocyanides (MeNC, Bu^{t}NC, *p*-MeC$_6$H$_4$NC or Bu^{n}NC) in tetrahydrofuran (thf) results in the loss of phosphine and thiol with reduction of the metal to give new metal(II) isocyanide complexes, for example as shown in equation (1)

$$[MoH(tipt)_3(PMePh_2)_n] + 4MeNC \xrightarrow{thf} cis\text{-}[Mo(tipt)_2(CNMe)_4] + Htipt + PR_3 \quad (1)$$

(M = Mo or W; RNC = MeNC or Bu^{t}NC; PR$_3$ = PMePh$_2$ or PMe$_2$Ph; *n* = 1 or 2). This method appears to be a very convenient general procedure for synthesis of such complexes. The reactions give green-brown solutions from which can be obtained, by addition of hexane, diamagnetic [Mo(tipt)$_2$(CNMe)$_4$] **1a**, [Mo(tipt)$_2$(CNBu^t)$_4$] **1b** and [W(tipt)$_2$(CNMe)$_4$] **1c** as amber-to-green crystalline solids. Reaction with Bu^{n}NC gave a brown solution from which no tractable solid could be obtained and although reaction with *p*-MeC$_6$H$_4$NC gave a brown solid it could not be satisfactorily characterised.

Selected physical and spectroscopic data for these compounds are listed in Table 1; other data are in the Experimental section. The complexes are monomeric in the solid state as shown by FAB mass spectrometry and the X-ray structural data discussed below. The infrared spectra of compounds **1** (Nujol mulls, Table 1) show CN stretching vibrations in the range 2150–1907 cm^{-1}. These values may be compared to those of the molybdenum(II) compounds [19,20] [Mo(CNMe)$_7$]$^{2+}$ and [Mo(CNBu^t)$_4$]$^{2+}$ which fall in the range 2140–2160 cm^{-1} and of the direct analogue *cis*-[Mo(Bu^{t}S)$_2$(CNBu^t)$_4$] [21] (2120, 2080 and 1997 cm^{-1}). Selected NMR data are shown in Table 1; the ^{1}H and ^{13}C spectra show the pairs of singlets expected from the two environments (axial and equatorial) of the isocyanide ligands.

We have determined the crystal structures of complexes **1** in order to gain further information on six-co-ordinate d^4 complexes which often show deformation from octahedral

Table 1 Physical and spectroscopic data for thiolateisocyanide complexes

Compound	Formula	Colour	$\tilde{\nu}$(CN)[a]/cm^{-1}	δ(^{1}H)[b] RNC	δ(^{1}H)[b] tipt	^3J(H–H)/Hz	δ(^{13}C)[b] M–*C*–NR
1a	$[Mo(tipt)_2(MeNC)_4]$	Amber	2149, 2067, 1907	3.7, 2.6	1.18 (d), 1.21 (d), 2.85 (sep), 3.81 (sep)	6.78	121.3, 152.1
1b	$[Mo(tipt)_2(Bu^tNC)_4]$	Emerald-green	2126, 2081, 2035	0.96, 1.50	1.21 (d), 2.81 (sep), 3.85 (sep)	6.77	124.0, 155.3
1c	$[W(tipt)_2(MeNC)_4]$	Green	2150, 2050, 1950	3.06, 4.07	1.22 (d), 2.84 (sep), 3.75 (sep)	6.84	127.1, 166.3

[a] Nujol mull spectra. [b] In CD_2Cl_2 solution, relative to $SiMe_4$; d = doublet, sep = septet.

Table 2 Selected molecular dimensions (lengths in Å, angles in °) in the complexes *cis*-$[M(SC_6H_2Pr^i_3\text{-}2,4,6)_2(CNR)_4]$ **1** with estimated standard deviations in parentheses

	1a M = Mo	**1c** M = W	**1b**	(Atoms in **1b**)
(*a*) About the metal atom				
M–S(1)	2.401(1)	2.395(2)	2.3942(7)	Mo–S
M–C(2)	2.086(5)	2.072(8)	2.083(2)	Mo–C(21)
M–C(3)	2.088(6)	2.082(9)	2.063(3)	Mo–C(16)
S(1)–M–S(1′)	117.9(1)	115.8(1)	121.07(4)	S–Mo–S′
S(1)–M–C(2)	87.8(2)	88.7(4)	91.80(7)	S–Mo–C(21)
S(1)–M–C(2′)	91.7(2)	92.5(4)	87.16(7)	S–Mo–C(21′)
S(1)–M–C(3)	158.0(1)	159.1(3)	155.11(7)	S–Mo–C(16′)
S(1)–M–C(3′)	82.8(1)	83.7(3)	83.30(7)	S–Mo–C(16)
C(2)–M–C(2′)	179.0(4)	177.8(12)	177.9(2)	C(21)–Mo–C(21′)
C(2)–M–C(3)	84.2(3)	82.8(7)	83.92(10)	C(21)–Mo–C(16′)
C(2)–M–C(3′)	96.6(3)	95.5(7)	97.80(10)	C(21)–Mo–C(16)
C(3)–M–C(3′)	77.9(2)	78.1(4)	73.07(14)	C(16)–Mo–C(16′)
(*b*) In the thiolate ligands				
S(1)–C(11)	1.797(6)	1.797(9)	1.791(2)	S–C(1)
M–S(1)–C(11)	112.7(2)	112.9(3)	113.45(8)	Mo–S–C(1)
(*c*) In the isocyanide ligands				
C(2)–N(21)	1.153(5)	1.170(10)	1.160(3)	C(21)–N(2)
N(21)–C(22)	1.419(6)	1.423(10)	1.451(3)	N(2)–C(22)
C(3)–N(31)	1.148(7)	1.144(11)	1.169(3)	C(16)–N(1)
N(31)–C(32)	1.422(8)	1.423(13)	1.455(4)	N(1)–C(17)
M–C(2)–N(21)	177.8(4)	172.8(26)	177.2(2)	Mo–C(21)–N(2)
C(2)–N(21)–C(22)	171.5(5)	169.6(16)	169.1(3)	C(21)–N(2)–C(22)
M–C(3)–N(31)	176.1(5)	177.1(10)	176.6(3)	Mo–C(16)–N(1)
C(3)–N(31)–C(32)	175.2(7)	173.5(13)	155.7(3)	C(16)–N(1)–C(17)

symmetry, mainly as a consequence of their electronic structure, although the overall complex geometry is also influenced by the properties of the ligands, *e.g.* steric hindrance, chelation, electronic effects, *etc*.[21] Hoffmann and co-workers[21–23] have classified such structures in terms of the variation in the angles between ligands in the equatorial plane of the idealised octahedron and this approach has been applied to classify d^4 thiolatecarbonyl complexes in terms of distortions from regular octahedral and regular trigonal-prismatic structures; a number of d^4 complexes have geometries between these two ideals.[3]

Molecular structure of *cis*-$[Mo(tipt)_2(CNMe)_4]$ 1a

The complex *cis*-$[Mo(tipt)_2(CNMe)_4]$ is thermally stable and is moderately stable to air in the solid state but is highly oxygen-sensitive in solution. It is soluble in most organic solvents except saturated hydrocarbons and crystallised from dichloromethane–hexane as yellow-brown (amber) rectangular prisms which were suitable for X-ray crystallography.

The molecular structure of this complex is shown in Fig. 1. Selected bond lengths and angles are in Table 2. In the crystal, the Mo atom lies on a two-fold symmetry axis. The two tipt ligands have a *cis* arrangement with a S–Mo–S′ angle of 117.9(1)°, increased from the 90° angle in a regular octahedron;

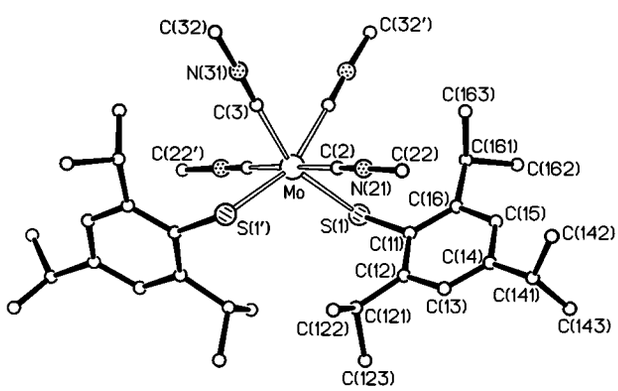

Fig. 1 View of a molecule of *cis*-$[Mo(tipt)_2(CNMe)_4]$ **1a**, showing the atomic numbering scheme. The crystal of the tungsten analogue, complex **1c**, is of the opposite enantiomer, having a structure virtually identical to the mirror image of that shown here. The two-fold symmetry axis is vertical in the plane of the paper

correspondingly, the opposite C–Mo–C′ angle is 77.9(2)°. The complex *cis*-$[Mo(SBu^t)_2(CNBu^t)_4]$[21] has a very similar geometry, the S–Mo–S and C–Mo–C angles being, respectively, 115.3(1) and 73.7(4)°. Also, *mer*-$[Mo(tipt)_2(CO)_3(PMePh_2)]$[3]

has S(1)–Mo–S(2) and C(3)–Mo–P(6) angles of 116.0(1) and 79.1(1)° respectively. With respect to the above data **1a** has octahedral geometry which is distorted somewhat, as characterised by the mean twist angle θ, estimated at 51° between one pair of opposing trigonal planes, each plane containing one sulfur atom and two carbon atoms (after normalisation of bond lengths); for a regular octahedron θ = 60° and for a regular trigonal prism θ = 0°. Compound **1a** can be classified therefore as a Class 1 complex according to the system described in ref. 3. The corresponding twist angle[3,21] for *cis*-$[Mo(SBu^t)_2(CNBu^t)_4]$ is 50°.

The metal–thiolate bond distance [2.401(1) Å] in compound **1a** is close to those observed in other six-co-ordinate molybdenum(II) thiolate complexes, {*e.g. mer*-$[Mo(tipt)_2(CO)_3(PMePh_2)]$[3] has *d*(Mo–S) = 2.380(1) and 2.366(1) Å, *cis*-$[Mo(SBu^t)_2(CNBu^t)_4]$[21] has *d*(Mo–S) = 2.374(3) and 2.372(3) Å and $[Mo(SBu^n)_2(dppe)_2]$ (dppe = $Ph_2PCH_2CH_2PPh_2$)[24] has *d*(Mo–S) = 2.361(1) Å} but it is longer than the value of 2.23 Å for the four-co-ordinate molybdenum(IV) compound $[Mo(SBu^t)_4]$.[25] The Mo–C distances [2.086(5) (mutually *trans*, or axial) and 2.088(6) (*trans* to the thiolate, or equatorial) Å] are, as expected, close to those of *cis*-$[Mo(SBu^t)_2(Bu^tNC)_4]$[21] [2.06(1) (axial) and 2.10(1) (equatorial) Å]. Less predictably, these distances are close to the Mo^{II}–C (isocyanide) distances in seven-co-ordinate compounds, *e.g.* 2.04–2.16 Å for the cation[19] $[Mo(CNMe)_7]^{2+}$. From the smaller co-ordination number in **1a** a shorter distance might have been expected.[26] Presumably the presence of the large S atoms in the co-ordination sphere has affected the Mo–C distance.

The two thiolate ligands are in the *anti* configuration, unlike the *syn* configuration seen for *cis*-$[Mo(SBu^t)_2(CNBu^t)_4]$.[21] This presumably reflects the larger steric requirement of the tipt ligands. The same *anti* configuration is seen for **1b** and **1c** (see below). In each of the three structures **1** the two thiolate ligands are related by a two-fold symmetry axis.

In the isocyanide ligands the C(2)–N(21) distance, 1.153(5) Å, is not significantly different from the C(3)–N(31) distance, 1.148(7) Å, and the angles C(2)–N(21)–C(22) and C(3)–N(31)–C(32) are 171.5(5) and 175.2(7)° respectively. Electron transfer to the isocyanide ligand through d_π–π* bonding should be reflected in its geometry, especially in the C≡N–C angle, but steric interactions can also have a major effect on this angle.[21] The analogue *cis*-$[Mo(SBu^t)_2(CNBu^t)_4]$ has a distinctly small C≡N–C angle of 160° for one of the axial ligands.[21] This small angle has been considered as most likely due to crystal-packing effects, as indicated by the close non-bonding contacts between the equatorial and the axial Bu^t groups.[21] These effects appear to be relatively small for compound **1a**.

Molecular structure of *cis*-$[Mo(tipt)_2(CNBu^t)_4]$ 1b

The five- and six-co-ordinate hydride complexes $[MoH(tipt)_3(PMePh_2)]$ and $[MoH(tipt)_3(PMe_2Ph)_2]$ reacted with an excess of Bu^tNC in thf under a dinitrogen atmosphere at room temperature to give *cis*-$[Mo(tipt)_2(CNBu^t)_4]$ **1b** which can be crystallised from dichloromethane–hexane as emerald-green crystals. The ^1H NMR spectrum shows two singlets for the Bu^tNC ligands as expected for the inequivalent isocyanide groups (Table 1), whereas *cis*-$[Mo(SBu^t)_2(CNBu^t)_4]$ shows only one sharp singlet for the Bu^tNC ligands, perhaps due to accidental degeneracy, since it shows the expected pairs of singlet Bu^t resonances in its ^{13}C spectrum.[21]

The molecular structure of **1b** is shown in Fig. 2 and selected bond lengths and angles are included in Table 2. Complex **1b** lies about a two-fold symmetry axis and has a distorted octahedral geometry with a wide S–Mo–S′ angle of 121.07(4)°, compared to the smaller angles of the groups C(16)–Mo–C(16′) 73.07(14) and S–Mo–C(16) 83.30(7)°. The best mean twist angle (θ) value for **1b**, estimated at 47°, is similar to that for **1a**.

The bond distance of the axial isocyanide carbons to the

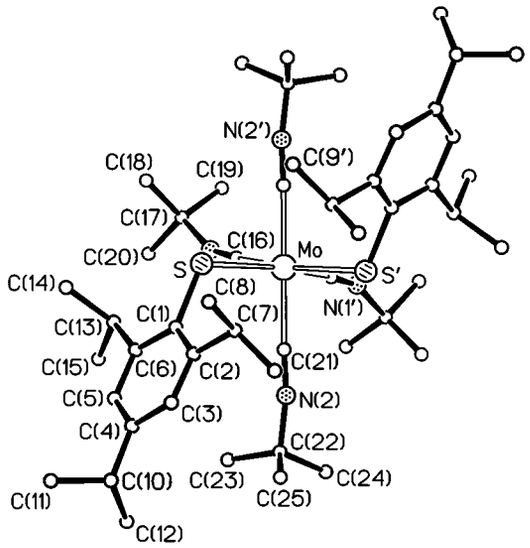

Fig. 2 A molecule of *cis*-$[Mo(tipt)_2(CNBu^t)_4]$ **1b**, viewed along the two-fold symmetry axis

Mo^{II} is a little longer than that of the equatorial ones [N(1)–C(16) 1.169(3) and N(2)–C(21) 1.160(3) Å]. The angles C≡N–C are more sensitive to electronic and packing effects and differ somewhat from each other, C(21)–N(2)–C(22) 169.1(3) and C(16)–N(1)–C(17) 155.7(3)°. These angles are notably smaller than corresponding angles in **1a** and closer to the small C≡N–C angle of 160° in the analogue *cis*-$[Mo(SBu^t)_2(Bu^tNC)_4]$ discussed above.[21] Presumably this is a consequence (steric and/or electronic) of the Bu^tNC ligands of **1b** as compared to MeNC in **1a**. Although the somewhat greater electron release from Bu^t compared to Me might influence the π character of the Mo–C–N system, the cause of the bond-angle difference is more likely to be steric than electronic.

Molecular structure of *cis*-$[W(tipt)_2(CNMe)_4]$ 1c

The green, diamagnetic complex *cis*-$[W(tipt)_2(CNMe)_4]$ **1c**, obtained from the reaction of $[WH(tipt)_3(PMe_2Ph)_2]$ with MeNC in thf, is very soluble in common solvents and moderately air-sensitive in the solid state. It was recrystallised from dichloromethane–hexane to produce green, square-prism crystals suitable for X-ray studies.

Compound **1c** was shown to be isostructural with the corresponding complex *cis*-$[Mo(tipt)_2(CNMe)_4]$ **1a**. The atomic coordinates generate a diagram virtually identical to the mirror image of Fig. 1; selected molecular dimensions are in Table 2. The W atom lies on a C_2 symmetry axis. The two tipt ligands in the *cis* arrangement have a S(1)–W–S(1′) angle of 115.8(1)° and the opposite C(3)–W–C(3′) angle is 78.1(4)°. Therefore complex **1c** is similarly distorted from regular octahedral geometry and is a member of Class 1 with a mean twist angle of *ca.* 53°.[3] The metal–thiolate bond distance, 2.395(2) Å, in **1c** is a little shorter than the Mo–S distance, 2.401(1) Å, in **1a**. The angle C(2)–N(21)–C(22) 169.6(16)° is smaller than C(3)–N(31)–C(32) 173.5(13)° and these values are slightly smaller than corresponding angles in **1a**. As in **1a**, there is little apparent steric or electronic effect operating which affects the WCNC system.

Electrochemical studies

At a platinum electrode at 25 °C in 0.2 M $[NBu_4][BF_4]$–CH_2Cl_2 complexes **1a** and **1b** exhibit by cyclic voltammetry a first (I) apparently single-electron, diffusion-controlled, reversible anodic wave at $^IE^\circ = -0.07$ V or -0.09 V *versus* the saturated calomel electrode (SCE), respectively ($i_{pa}/i_{pc} \approx 1.0$, $\Delta E_p \approx 80$ mV, roughly constant current function $i_p^{-1}C^{-1}$ for the scan rate range from 50 mV s^{-1}). This is followed, at a higher potential

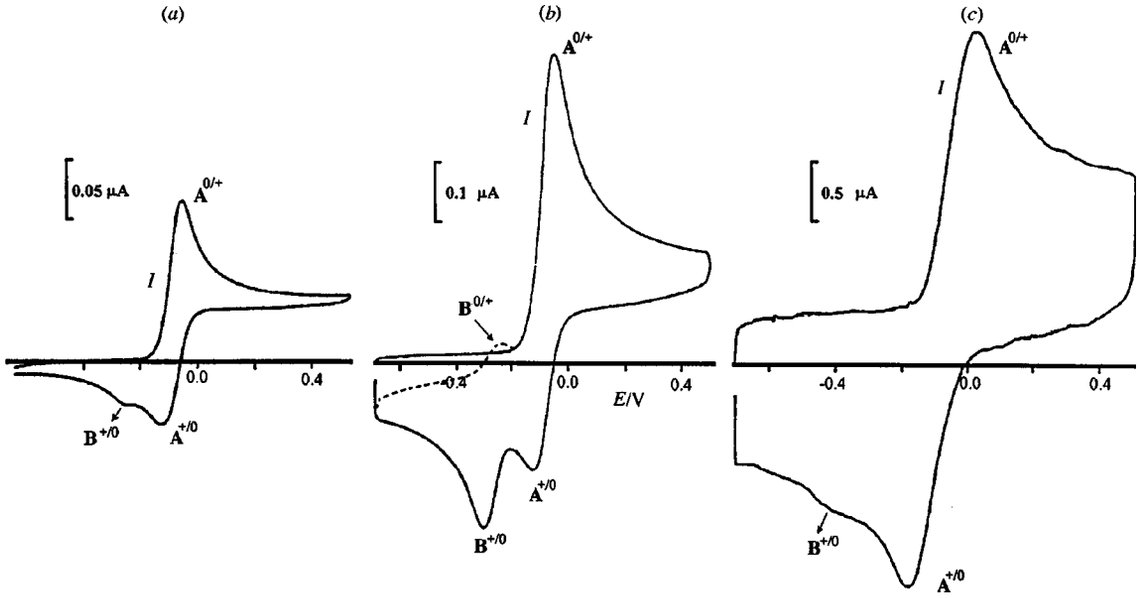

Fig. 3 Cyclic voltammograms of *cis*-[Mo(tipt)$_2$(CNBu^t)$_4$] (1.13 mM, in CH_2Cl_2 with 0.2 M [NBu_4][BF_4]) at −50 °C and at a platinum-disc (d = 0.5 mm) working electrode. Potentials are given in V *vs.* SCE; **A** and **B** denote the *cis* and *trans* isomers, respectively (see text). Scan rate: 0.05 (*a*), 0.8 (*b*) and 20 V s^{-1} (*c*)

($^{II}E_p$ = 1.03 or 1.09 V, respectively, measured at 200 mV s^{-1}), by a second (II) irreversible anodic wave.

However, in the electrolyte medium, the complexes are unstable and the above anodic waves are progressively replaced by two others at higher potentials, the first one (at E° = 0.50 or 0.30 V for **1b** or **1a** respectively) being reversible and the second (at E_p^{ox} *ca.* 1.3 V) irreversible [*e.g.* for **1b**, ≈35% conversion into the decomposition product (X) was detected after about 30 min and full conversion was achieved after *ca.* 5 h]. In this respect we note that the analogous complex *cis*-[Mo(SBu^t)$_2$(CNBu^t)$_4$] in dimethylformamide was reported to have a one-electron reduction at E° = −0.17 V and an oxidation at E° = 0.45 V *versus* SCE.[21] However, on the basis of the above observations for **1a** and **1b**, we consider that the first process is in fact a one-electron *oxidation* of *cis*-[Mo(SBu^t)$_2$(CNBu^t)$_4$] and the second process is due to the oxidation of a decomposition product.

Owing to the instability of compounds **1a** and **1b** in solution, their exhaustive controlled-potential electrolysis (CPE) at a potential (0.15 V) on the plateau of the anodic wave (I) consumes much less than 1 F mol^{-1} (*e.g.* ≈0.3 F mol^{-1} for **1b**) due to the spontaneous conversion, during the time of the electrolysis, of the starting complex into a derived product of decomposition (X, see above) which is not redox active at the applied potential. [It can only be oxidised at a higher potential than that of the CPE at wave (I).] In agreement with this interpretation, if a second CPE (*i.e.* following the above CPE) is carried out on the plateau (≈0.6 V) of the wave of this derived product (X) a transfer of 0.5 e per molecule of initial complex is measured. This gives a total number of electrons of 0.8 for the first waves of the initial complex and the product of decomposition. Presumably a further decomposition process of X accounts for the remaining 0.2 e.

In view of the decomposition of compounds **1a** and **1b**, which hinders a detailed investigation of their electrochemical behaviour at ambient temperatures, we have performed a detailed electrochemical study, most thoroughly for **1b**, at −50 °C, a temperature at which no decomposition was detected for periods up to 24 h. Moreover, an interesting behaviour was observed at the first anodic wave (I). When the potential scan is inverted after this wave two reduction waves are detected (see Fig. 3). One of these is the cathodic component counterpart of the anodic wave. The other one, at a lower potential, corresponds to the reduction of another species (which we denote as

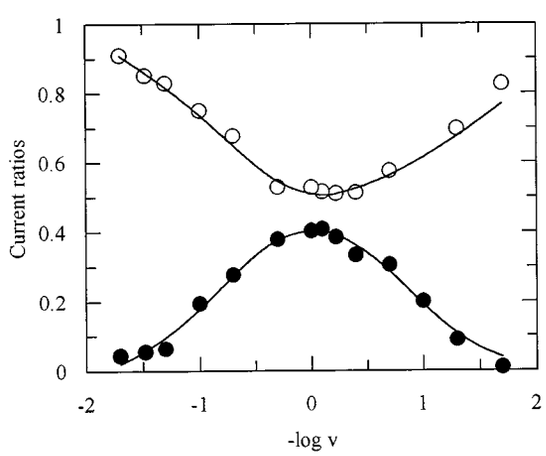

Fig. 4 Experimental (symbols) and theoretical (lines) variations of the reversibility of wave (I), $i_p(cis^{+/0})/i_p(cis^{0/+})$, (top) and of the parameter $\rho = i_p(trans^{+/0})/i_p(cis^{0/+})$ (bottom) as a function of scan rate. The solid lines correspond to the working curves for the mechanism described in Scheme 1 where k_1 = 5, k_{-1} = 2.5, k_{-2} = 1 and k_2 = 0 s^{-1}

B$^+$) which is generated at the anodic process of the starting complex, whether **1a** or **1b**, which we simply denote as **A**. The new cathodic wave has an anodic counterpart, thus forming a reversible redox pair **B**$^+$/**B**. This is observed upon scan reversal and these redox waves are detected only after scanning the potential over that of the anodic wave of **A**.

This behaviour is rather dependent on the scan rate, although the current function of the anodic peak current (**A** oxidation) is constant over the entire scan rate range (from 20 mV s^{-1} up to 50 V s^{-1}) indicating the involvement of a constant number of electrons in the anodic process. For a sufficiently high (> ≈ 50 V s^{-1}), or low (< ≈ 20 mV s^{-1}) scan rate the cathodic component of the anodic wave of **A** is the only observed cathodic wave upon scan reversal [Fig. 3(*a*) and 3(*c*) correspond to situations approaching these limits]; the redox wave thus appears to correspond to a single-electron, reversible process (**A**$^+$/**A**).

The new cathodic wave (**B**$^+$ reduction) is detected at intermediate scan rates and its relative intensity, $\rho = i_p(\mathbf{B}^{+/0})/i_p(\mathbf{A}^{0/+})$, passes through a maximum at ≈1.0 V s^{-1} [see Fig. 4 (symbols) and 5(*a*)]; moreover, its formation occurs at the expense of the cathodic counterpart of the anodic wave of **A**, *i.e.*

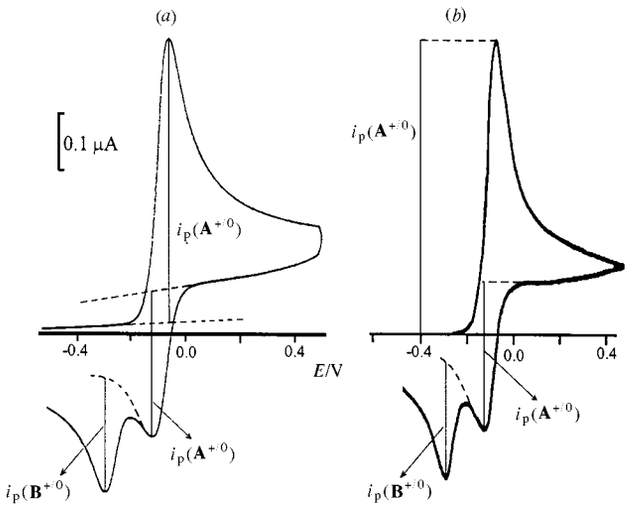

Fig. 5 Experimental (*a*) and simulated (*b*) (according to the mechanism in Scheme 1 where $k_1 = 5$, $k_{-1} = 2.5$, $k_{-2} = 1$ and $k_2 = 0$ s^{-1}) cyclic voltammograms at 0.8 V s^{-1} of a solution of *cis*-[Mo(tipt)$_2$(CNBu^t)$_4$] (see conditions in Fig. 3), showing the extrapolated curves for the measurements of the required peak currents

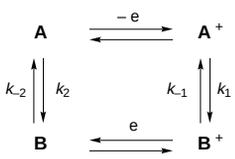

Scheme 1

$i_p(A^{+/0})/i_p(A^{0/+})$ varies *inversely* with ρ and attains its minimum value at the maximum value of ρ.

These observations can be interpreted by considering an electrochemical–chemical square-type process (Scheme 1), in which $E^\circ(A^{+/0}) = -0.09$ V and $E^\circ(B^{+/0}) = -0.27$ V *versus* SCE (for **1b**). Thus the high-scan-rate limiting behaviour corresponds to the simple reversible single-electron oxidation of **A**, since there is no time for the occurrence of appreciable conversion of A^+ into B^+. However, upon decreasing the scan rate, a partial and increasing conversion of A^+ into B^+ occurs and increasing relative amounts of the latter species are detected by monitoring its cathodic wave (increasing ρ). Nevertheless, ρ passes through a maximum and then starts to decrease on lowering the scan rate. This can be accounted for by considering that during the slow reverse scan A^+ is reduced before B^+ [$E^\circ(A^{+/0}) > E^\circ(B^{+/0})$], thus shifting the B^+/A^+ equilibrium towards the **A** side. There is sufficient time for extensive conversion of B^+ into A^+ before onset of reduction of B^+; therefore, the intensity of the cathodic $A^{+/0}$ wave tends to that expected for a reversible single-electron process, whereas that for the cathodic wave of B^+ decreases. No significant variation of the above behaviour was detected upon changing the concentration of the complex, thus suggesting the involvement of first-order chemical steps.

The mechanism of Scheme 1 was investigated in detail for compound **1b** by digital simulation (program CVSIM[27]) of the cyclic voltammograms at different scan rates (in the 0.02–50 V s^{-1} range). An excellent fit was obtained for the following rate constant values: $k_1 = 5$, $k_{-1} = 2.5$, $k_{-2} = 1$ and $k_2 \leqslant k_{-2}$ (*i.e.* $k_{-2} \approx 0$ s^{-1}). This is illustrated in Fig. 5 for the scan rate of 0.8 V s^{-1} (the procedure was applied successfully at regular scan rate intervals over all the above range), and is also shown by the plot (Fig. 4) of the experimental (symbols) and simulated (lines) current ratios $\rho = i_p(B^{+/0})/i_p(A^{0/+})$ and $i_p(A^{+/0})/i_p(A^{0/+})$ as a function of scan rate.

The low value of the rate constant k_2 can also be estimated (1.7×10^{-4} s^{-1}) by considering that $\Delta G^\circ = 0$ along the thermochemical cycle of Scheme 1. This condition leads upon rearrangement to expression (2) which relates the chemical

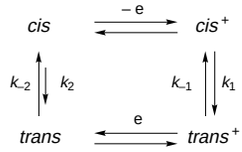

Scheme 2

$$\ln(K_1/K_2) = \frac{F}{RT}[E^\circ(A^{+/0}) - E^\circ(B^{+/0})] \qquad (2)$$

equilibrium constants $K_1 = k_1/k_{-1}$ and $K_2 = k_2/k_{-2}$, and from which k_2 can be estimated since k_1, k_{-1}, k_{-2} and the oxidation potentials are already known (see above).

Hence, the equilibrium $A \rightleftharpoons B$ lies very much in favour of **A** ($K_2 = 1.7 \times 10^{-4}$) in agreement with the fact that the anodic wave of **A** is the only one detected during the anodic scan. However, oxidation of **A** to A^+ promotes thermodynamically its conversion into the new species (B^+) ($K_1 = 2$); moreover, the kinetics is also accelerated upon oxidation, therefore the conversion into the more stable species is faster at the cationic 15-electron level than at the neutral 16-electron level, *i.e.* $k_1(A^+ \longrightarrow B^+) = 5$ $s^{-1} > k_{-2}$ ($B \longrightarrow A$) = 1 s^{-1}.

These observations follow the behaviour also recognised[7,9,15] for some 18-/17-/16-electron octahedral phosphine-ligated systems with carbonyl or nitrile coligands. These, upon oxidation, undergo *cis*-to-*trans* isomerisation; the derived *trans* isomers have redox potentials at lower values than those of the corresponding *cis* isomers.

A further point worthy of discussion is the nature of the derived species B^+. In view of the high similarity of the electrochemical behaviour between our complexes and those which undergo anodically induced *cis*-to-*trans* isomerisation noted above, we propose that a similar geometric isomerisation is occurring in the present systems, *i.e.* the redox $B^{+/0}$ pair corresponds to *trans*-[Mo(tipt)$_2$(CNR)$_4$]$^{+/0}$.

As further circumstantial evidence, we note that the free-energy variation associated with the K_2 chemical reaction of our system ($\Delta G_2^\circ = 3.9$ kcal mol^{-1}; cal = 4.184 J) is much higher than that (0.007 kcal mol^{-1}) estimated,[21] in the model compound [Mo(SH)$_2$(CNH)$_4$], for the energy difference between the *syn* and the *anti* conformers. Moreover, it is lower than the energy (*ca.* 15 kcal mol^{-1})[21] required to convert any of these conformers into the less stable 'in-plane' ones. Therefore, our chemical transformation can be expected to involve a process which is more complex than simple conversion between the *syn* and *anti* conformers, but not so energetically demanding as one involving conversion to 'in-plane' conformers, which in our case would have a considerable steric barrier and would therefore be unlikely to occur. Hence, the *cis*-to-*trans* isomerisation we are proposing is the most plausible redox-induced transformation for our complexes, and Scheme 1 therefore can assume the form depicted in Scheme 2.

To our knowledge, this study provides the first detailed kinetic investigation of such a redox-induced process in a 16-/15-electron system.

Experimental

Syntheses

The compounds Htipt,[28] [WH(tipt)$_3$(PMe$_2$Ph)$_2$],[29] [MoH(tipt)$_3$(PMePh$_2$)],[2,30] [MoH(tipt)$_3$(PMe$_2$Ph)$_2$][29] and MeNC[31] were prepared by published methods; Bu^{t}NC and *p*-MeC$_6$H$_4$NC were used as purchased from Aldrich Chemical Co.

All manipulations were carried out under a dinitrogen atmosphere using conventional Schlenk-tube and syringe or

glove-box techniques. Reaction solvents were dried and freshly distilled under dinitrogen. The NMR spectra were measured using a JEOL FX270 spectrometer, infrared spectra on a Perkin-Elmer 883 spectrometer and fast atom bombardment (FAB) mass spectra with a VG70-2505 spectrometer, using a xenon flux. Elemental analyses were carried out by the Microanalytical Services Department, University of Surrey, or by Butterworth Analytical Laboratories, Ltd.

***cis*-Tetrakis(methyl isocyanide)bis(2,4,6-triisopropylbenzenethiolato)molybdenum(II) 1a.** *Method A.* To a green solution of $[MoH(tipt)_3(PMePh_2)]$ (0.41 g, 0.45 mmol) in thf (40 cm^3) was added freshly distilled MeNC (0.7 cm^3, excess). The solution was stirred at room temperature for 30 min. The resulting red-brown solution was evaporated to dryness under vacuum and the residue kept under vacuum for 2 h. Addition, under nitrogen, of hexane (20 cm^3) gave a yellow powder that was filtered off and washed with hexane (2 × 5 cm^3). Crystallisation of the product by slow diffusion of hexane into a dichloromethane solution at room temperature produced yellow-brown single crystals (0.26 g, 89% yield).

Method B. The compound $[MoH(tipt)_3(PMe_2Ph)_2]$ and methyl isocyanide were allowed to react as in method A to produce $[Mo(tipt)_2(CNMe)_4]$ (yield 71%) (Found: C, 61.6; H, 7.9; N, 7.8. Calc. for $C_{38}H_{58}MoN_4S_2$: C, 62.3; H, 8.0; N, 7.7%).

***cis*-Tetrakis(*tert*-butyl isocyanide)bis(2,4,6-triisopropylbenzenethiolato)molybdenum(II) 1b.** *Method A.* The compound $[MoH(tipt)_3(PMePh_2)]$ (0.41 g, 0.4 mmol) in thf (40 cm^3) was treated with $CNBu^t$ (0.88 g, 10 mmol). The mixture was stirred for 1.5 h, during which time it changed from green to dark green. The solvent was removed *in vacuo* and the residue dried under vacuum for 1 h. Hexane (10 cm^3) was added and the product was obtained as a pea-green powder after stirring for 20 min. It was filtered off and washed with hexane (2 × 5 cm^3). Crystallisation by slow diffusion of layered hexane over a CH_2Cl_2 solution produced emerald-green crystals (yield 66%) (Found: C, 66.5; H, 9.0; N, 6.1. Calc. for $C_{50}H_{82}MoN_4S_2$: C, 66.8; H, 9.2; N, 6.2%). FAB mass spectrum: *m*/*z*, 817 $[M - CNBu^t]^+$ (M^+, calc. 899.3).

Method B. Analogous to the above procedure, $[MoH(tipt)_3(PMe_2Ph)_2]$ and Bu^tNC reacted to produce *cis*-$[Mo(tipt)_2(CNBu^t)_4]$ (yield 76%).

***cis*-Tetrakis(methyl isocyanide)bis(2,4,6-triisopropylbenzenethiolato)tungsten(II) 1c.** The complex $[WH(tipt)_3(PMe_2Ph)_2]$ (0.15 g, 0.24 mmol) was dissolved in thf (*ca.* 30 cm^3) under a nitrogen atmosphere. Methyl isocyanide (0.7 cm^3, excess) was added and the mixture stirred for 2 h at room temperature. The solvent was evaporated to dryness under vacuum and the product obtained as a pea-green powder by addition of hexane (10 cm^3). It was filtered off and washed with hexane (2 × 5 cm^3). Crystallisation by slow diffusion of layered hexane over a solution in dichloromethane at room temperature produced bright green crystals (yield 68%) suitable for X-ray crystallographic analysis (Found: C, 54.9; H, 7.1; N, 6.1. Calc. for $C_{38}H_{58}N_4S_2W$: C, 55.7; H, 7.1; N, 6.8%). FAB mass spectrum: *m*/*z*, 777 $[M - CNMe]^+$ (M^+, calc. 818.9).

Reaction of hydrido(methyldiphenylphosphine)tris(2,4,6-triisopropylbenzenethiolato)molybdenum(IV) with *p*-tolyl isocyanide and *n*-butyl isocyanide. The compound $[MoH(tipt)_3(PMePh_2)]$ and *p*-MeC_6H_4NC reacted as for $[Mo(tipt)_2(MeNC)_4]$ above, except that in this experiment pentane was used in place of hexane. The crude product, $[Mo(tipt)_2(p\text{-}MeC_6H_4NC)_4]$, was obtained in 68% yield but could not be obtained analytically pure. A similar reaction using Bu^nNC gave only an intractable oil.

Crystallography

***cis*-$[Mo(tipt)_2(CNMe)_4]$ 1a.** *Crystal data.* $C_{38}H_{58}MoN_4S_2$, $M = 731.0$, monoclinic, space group $C2$ (no. 5), $a = 16.143(1)$, $b = 15.311(2)$, $c = 8.5933(5)$ Å, $\beta = 107.073(5)°$, $U = 2030.3(3)$ $Å^3$, $Z = 2$, $D_c = 1.196$ g cm^{-3}, $F(000) = 776$, μ(Mo-Kα) = 4.4 cm^{-1}, λ(Mo-Kα) = 0.71069 Å, $T = 293$ K.

Crystals are small, amber, rectangular prisms. One, *ca.* 0.12 × 0.14 × 0.19 mm, was mounted on a glass fibre and coated with epoxy resin. After photographic examination showing fine, sharp diffraction spots, the crystal was transferred to an Enraf-Nonius CAD4 diffractometer (with monochromated radiation) for determination of accurate cell parameters (by refinement from the settings of 25 reflections, θ *ca.* 10.5°, each reflection centred in four orientations) and for measurement of diffraction intensities (to θ_{max} 25°).

During processing, intensities were corrected for Lorentz-polarisation effects, absorption (by semiempirical ψ-scan methods) and to remove negative net intensities (by Bayesian statistical methods). Of 1861 unique reflections entered into the SHELX system,[32] 1721 were 'observed', having $I > 2\sigma_I$.

The structure was determined by the heavy-atom method and refined by full-matrix least-squares methods. Hydrogen atoms were included in idealised positions; the phenyl and methine H atoms were set to ride on their parent carbon atoms, and the methyl H atoms were refined with geometrical constraints. The isotropic thermal parameters of all H atoms were refined freely. The non-hydrogen atoms were allowed anisotropic thermal parameters. At the conclusion of the refinement procedure, $R = 0.041$ and $R_g = 0.035$[32] for all 1861 reflections weighted $w = (\sigma_F)^{-2}$. Refinement of the structure with the opposite polarity showed very little difference. In the final difference map the highest peaks, *ca.* 0.37 e $Å^{-3}$, were close to the Mo atom.

Scattering factor curves for neutral atoms were taken from ref. 33. Computer programs used in this analysis have been noted above and in Table 4 of ref. 34, and were run on the DEC MicroVAX 3600 computer in the Nitrogen Fixation Laboratory.

***cis*-$[Mo(tipt)_2(CNBu^t)_4]$ 1b.** *Crystal data.* $C_{50}H_{82}MoN_4S_2$, $M = 899.3$, monoclinic, space group $C2/c$ (no. 15), $a = 18.560(4)$, $b = 16.598(3)$, $c = 19.156(6)$ Å, $\beta = 116.55(3)°$, $U = 5279(2)$ $Å^3$, $Z = 4$, $D_c = 1.13$ Mg m^{-3}, $F(000) = 1936$, μ(Mo-Kα) = 3.6 cm^{-1}, λ(Mo-Kα) = 0.71069 Å, $T = 173(2)$ K.

Slow diffusion of layered hexane over a CH_2Cl_2 solution of *cis*-$[Mo(tipt)_2(Bu^tNC)_4]$ resulted in large emerald-green crystals. The crystal for analysis was cut to 0.40 × 0.40 × 0.20 mm, mounted on a glass fibre and coated with paraffin. It was transferred to an Enraf-Nonius CAD4 diffractometer (with monochromated radiation). Accurate cell dimensions were determined using the 25 strongest independent reflections with θ between 6 and 10°, each reflection centred in four different orientations of the reflection plane. From the intensity measurements the crystal system and space group were determined. For the structure analysis a total of 6362 unique reflections, of which 5022 had $I > 2\sigma$, were measured to $\theta_{max} = 28°$.

Lorentz-polarisation corrections were used but a decay correction was not applied. A correction for absorption (T_{max} 1.00, T_{min} 0.93) was applied based on ψ-scan measurements. The structure was solved using heavy-atom methods with the SHELXS 86 program.[35] The refinement was carried out using full-matrix least-squares methods with the SHELXL 93 program.[36] The Mo, S, N and C atoms were refined anisotropically. The hydrogen atoms were placed in idealised positions with thermal parameters U_{iso} and allowed to ride with the parent atom ($U_{iso} = 1.2\ U_{eq}$ for C atoms or 1.5 U_{eq} for methyl groups).

The final refinement resulted in an $R1$ factor of 0.064 [for $I > 2\sigma(I)$] and $wR2$ of 0.097 (for all 6362 reflections), weighted $w = (\sigma_F)^{-2}$.

***cis*-[W(tipt)$_2$(CNMe)$_4$] 1c.** *Crystal data.* $C_{38}H_{58}N_4S_2W$, M = 818.9, monoclinic, space group $C2$ (no. 5), a = 16.138(1), b = 15.350(2), c = 8.6227(5) Å, β = 107.331(6)°, U = 2039.0(3) Å^3, Z = 2, D_c = 1.334 g cm^{-3}, $F(000)$ = 840, μ(Mo-Kα) = 30.2 cm^{-1}, λ(Mo-Kα) = 0.71069 Å, T = 293 K.

Crystals are green, square prisms. One, *ca*. 0.12 × 0.14 × 0.26 mm, was mounted on a glass fibre and coated with grease. The crystallographic analysis follows closely that described for the isostructural complex **1a** above. During processing, intensity data were corrected additionally for crystal deterioration (16% overall). 1867 Unique reflections (1829 of which had $I > 2\sigma_I$) were input to the SHELX system.[32]

The structure was confirmed by taking the atomic parameters directly from the analogous molybdenum complex. Refinement by full-matrix least-squares methods yielded final R and R_g indices of 0.035 and 0.034 for all 1867 reflections, weighted $w = 1/(\sigma_F^2 + 0.000\,157F^2)$. In the final difference map, the four largest peaks, 0.5–0.70 e Å^{-3}, were all close to the W atom.

Refinement of the structure with the opposite polarity gave significantly higher indices, *viz*. R = 0.041 and R_g = 0.045 for all data weighted $w = (\sigma_F^2 + 0.000\,43F^2)^{-1}$.

CCDC reference number 186/681.

Electrochemistry

The electrochemical experiments were performed on an EG & G PARC 273 potentiostat/galvanostat connected to a personal computer through a GPIB interface (National Instruments PC-2A) or on an EG & G PARC 173 potentiostat/galvanostat and an EG & G PARC 175 Universal programmer, in the Centro de Química Estrutural. Cyclic voltammetry, steady-state voltammetry at an ultramicroelectrode and chronoamperometry were undertaken in a two-compartment three-electrode cell, at a platinum-disc working electrode (d = 0.5 mm, 12.5 μm or 1.0 mm, respectively), probed by a Luggin capillary connected to a silver-wire pseudo-reference electrode; a platinum auxiliary electrode was employed. Controlled-potential electrolysis was carried out in a two-compartment three-electrode cell with platinum-gauze working and counter electrodes in compartments separated by a glass frit; a Luggin capillary, probing the working electrode, was connected to a silver-wire pseudo-reference electrode. The electrochemical experiments were performed in a nitrogen atmosphere both at room temperature and at −50 °C. The potentials were measured in 0.2 M $[NBu_4][BF_4]$–CH_2Cl_2 and are quoted relative to the saturated calomel electrode (SCE) by using as internal reference the $[Fe(\eta^5\text{-}C_5H_5)_2]^{+/0}$ couple (E° = 0.53 V *vs*. SCE).

The mechanism of the redox-induced isomerisation was investigated by simulation (program CVSIM[27]) of the voltammograms at different scan rates (in the 0.02–50 V s^{-1} range) and various concentrations of the complex. For simulation purposes, the transfer coefficient (α) was assumed to be 0.5 in all cases. The diffusion coefficient of the complex **1b**, at −50 °C, was estimated as 6 × 10^{-7} cm^2 s^{-1} by chronoamperometry and steady-state voltammetry at an ultramicroelectrode by using ferrocene as a reference compound[37] and this value was used for the diffusion coefficients of **A**, **A**$^+$, **B** and **B**$^+$ in the simulations.

The determination of the current ratios for both the experimental and theoretical voltammograms was performed (Fig. 5) as indicated previously.[9]

Acknowledgements

We thank the Junta Nacional de Investigaçåo Cientifica e Technológica/British Council protocol of collaboration, the PRAXIS XXI programme and the BBSRC for support. K. M. thanks the Ministry of Culture and Higher Education of the Islamic Republic of Iran for a maintenance grant.

References

1 T. E. Burrow, A. Hills, D. L. Hughes, J. D. Lane, R. H. Morris and R. L. Richards, *J. Chem. Soc*., *Dalton Trans*., 1991, 1813 and refs. therein.
2 D. L. Hughes, N. J. Lazarowych, M. J. Maguire, R. H. Morris and R. L. Richards, *J. Chem. Soc*., *Dalton Trans*., 1995, 5.
3 T. E. Burrow, D. L. Hughes, A. J. Lough, M. J. Maguire, R. H. Morris and R. L. Richards, *J. Chem. Soc*., *Dalton Trans*., 1995, 1315.
4 D. L. Hughes, K. Marjani and R. L. Richards, *J. Organomet. Chem*., 1995, **505**, 127.
5 T. E. Burrow, D. L. Hughes, A. J. Lough, M. J. Maguire, R. H. Morris and R. L. Richards, *J. Chem. Soc*., *Dalton Trans*., 1995, 2583.
6 W. E. Geiger, in *Prog. Inorg. Chem*., 1985, **33**, 275.
7 A. M. Bond, R. Colton, J. B. Cooper, J. C. Traeger, J. N. Walter and D. M. Way, *Organometallics*, 1994, **13**, 3434; A. M. Bond, B. S. Grabaric and J. J. Jacowski, *Inorg. Chem*., 1978, **17**, 2153 and refs. therein.
8 M. Menon, A. Pramanik, N. Bag and A. Chakravorty, *J. Chem. Soc*., *Dalton Trans*., 1995, 1543.
9 M. F. C. Guedes da Silva, J. J. R. Fraústo da Silva, A. J. L. Pombeiro, C. Amatore and J.-N. Verpeaux, *Organometallics*, 1994, **13**, 3943.
10 T. A. George, J. R. D. Debord, B. B. Kaul, C. J. Pickett and D. J. Rose, *Inorg. Chem*., 1992, **31**, 1295.
11 T. Adachi, M. C. Durrant, D. L. Hughes, C. J. Pickett, R. L. Richards, J. Talarmin and T. Yoshida, *J. Chem. Soc.*, *Chem. Commun*., 1992, 1464.
12 G. Barrado, G. A. Carriedo, C. Diaz-Valenzuela and V. Riera, *Inorg. Chem*., 1991, **30**, 4416.
13 F. C. Anson, T. J. Collins, S. L. Gipson, J. T. Keech, T. E. Knafft and G. T. Peake, *J. Am. Chem. Soc*., 1986, **108**, 6593.
14 K. A. Conner and R. A. Walton, *Inorg. Chem*., 1986, **25**, 4422.
15 A. Vallat, M. Person, L. Roullicle and E. Laviron, *Inorg. Chem*., 1987, **26**, 332.
16 B. E. Bursten, *J. Am. Chem. Soc*., 1982, **104**, 1299.
17 J. N. Murrell, A. Al-Derzi, G. J. Leigh and M. F. Guest, *J. Chem. Soc*., *Dalton Trans*., 1980, 1425.
18 D. L. Dubois and R. Hoffmann, *Nouv J. Chim*., 1977, **1**, 479.
19 P. Brant, F. A. Cotton, J. C. Sekutowski, T. E. Wood and R. A. Walton, *J. Am. Chem. Soc*., 1979, **101**, 6588.
20 E. I. Stiefel, *Prog. Inorg. Chem*., 1977, **22**, 1.
21 M. Kamata, K. Hirotsu, T. Higuchi, K. Tastsumi, R. Hoffmann, T. Yoshida and S. Otsuka, *J. Am. Chem. Soc*., 1981, **103**, 5772.
22 R. Hoffmann, J. M. Howell and A. R. Rossi, *J. Am. Chem. Soc*., 1976, **98**, 2484.
23 P. Kubacek and R. Hoffmann, *J. Am. Chem. Soc*., 1981, **103**, 4320.
24 C. A. Shortman, D. Povey and R. L. Richards, *Polyhedron*, 1986, **5**, 369.
25 S. Otsuka, M. Kamata, K. Hirotsu and T. Higuchi, *J. Am. Chem. Soc*., 1981, **103**, 3011.
26 J. Hyde, L. Magin and J. Zubieta, *J. Chem. Soc.*, *Chem. Commun*., 1980, 204.
27 D. K. Gosser, jun. and F. Zhang, *J. Electroanal. Chem. Interfacial Electrochem*., 1991, **38**, 715.
28 P. J. Blower, J. R. Dilworth, J. P. Hutchinson and J. A. Zubieta, *J. Chem. Soc*., *Dalton Trans*., 1985, 1533.
29 T. E. Burrow, D. L. Hughes, A. Hills, A. J. Lough, J. D. Lane, R. H. Morris and R. L. Richards, *J. Chem. Soc*., *Dalton Trans*., 1991, 2519.
30 T. E. Burrow, A. Hills, D. L. Hughes, N. J. Lazarowych, M. J. Maguire, J. D. Lane, R. H. Morris and R. L. Richards, *J. Chem. Soc.*, *Chem. Commun*., 1990, 1757.
31 R. E. Schuster, J. E. Scott and J. Casanova, *Org. Synth*., 1966, **46**, 75.
32 G. M. Sheldrick, SHELX, Program for crystal structure determination, University of Cambridge, 1976; also SHELXN, an extended version of SHELX, 1977.
33 *International Tables for X-Ray Crystallography*, Kynoch Press, Birmingham, 1974, vol. 4, pp. 99 and 149.
34 S. N. Anderson, R. L. Richards and D. L. Hughes, *J. Chem. Soc*., *Dalton Trans*., 1986, 245.
35 G. M. Sheldrick, SHELXS 86, Program for the solution of crystal structures, University of Göttingen, 1985.
36 G. M. Sheldrick, SHELXL 93, Program for crystal structure refinement, University of Göttingen, 1993.
37 C. Amatore, M. Azzabi, P. Callas, A. Justand, C. Lefrou and Y. Rollin, *J. Electroanal. Chem. Interfacial Electrochem*., 1990, **45**, 45.

Received 3*rd June* 1997; *Paper* 7/03860C